Synthesis of Ultra-small ZnS Nanoparticles by Solid−Solid Reaction in the Confined Space of AOT Reversed Micelles

Pietro Calandra,[†] Alessandro Longo,[‡] and Vincenzo Turco Liveri*,[†]

Dipartimento di Chimica-Fisica, Università degli Studi di Palermo, Viale delle Scienze Parco d'Orleans II, 90128 Palermo, Italy, and ISMN, Istituto per lo Studio dei Materiali Nanostrutturati, Via Ugo La Malfa 153, 90146 Palermo, Italy

Received: May 16, 2002; In Final Form: August 13, 2002

Ultra-small ZnS nanoparticles have been synthesized by a novel solid−solid reaction between Na_2S and $ZnSO_4$ nanoparticles in the confined space of AOT reversed micelles. The reaction was performed by mixing two dry AOT/*n*-heptane solutions, containing Na_2S and $ZnSO_4$ nanoparticles, respectively. This synthetic route has been revealed to have specific advantages giving anhydrous systems with high nanoparticle concentration. From these systems, by simple evaporation of the organic solvent, interesting AOT/ZnS composites can be prepared. Size, polydispersity, and photophysical properties of AOT reversed micelles containing ZnS nanoparticles dispersed in *n*-heptane have been investigated as function of salt and AOT concentrations by SAXS and UV spectroscopy. The UV spectra of all samples, including AOT/ZnS composites, showed a red shift of the first excitonic transition band with time but, as assured by SAXS experiments performed on liquid samples, this phenomenon was not associated with any change in mean size and/or polydispersity of ZnS containing AOT reversed micelles.

Introduction

Solid-state reactions involve the blending of solid phase reactants, usually in the form of fine powders to speed up the process, and the chemical reaction occurs without the help of any solvent. In such condition, the reaction path and, consequently, the products can be different from those of the same reaction in solution.[1] This could open new directories for modern synthetic chemistry where the possibility of obtaining new materials is, in fact, of crucial importance. Many examples of solid-state reactions of technological interest, including redox reactions, couplings, and rearrangements, can be found in refs 2−6.

Generally the major drawbacks of all solid-state reactions are the slowness and the fact that they are usually not quantitative, since the reaction involves only interfacial atoms and the diffusion of chemical species is negligible in the solid phase. Although extremely slow solid-state reactions can be investigated by special techniques,[7] they are not generally useful for practical applications, so the most common expedient to speed up the reaction[4,8,9] is to increase the reaction temperature, even up to 1000−1500 °C.

The use of very small particles dispersed in a suitable liquid medium appears to be an alternative solution to the aforementioned problems since they are characterized by a high fraction of surface reactive atoms, thus avoiding the use of drastic and economically disadvantageous conditions such as high pressure and/or high temperature. Hence the idea inspiring this paper is to exploit high surface-to-volume ratio particles dispersed in reversed micellar systems, as reacting solid particles to perform solid−solid reactions at mild conditions. In this way, because the fraction of surface atoms and their reactivity are quite high, the solid-phase reaction should occur quickly and quantitatively. Moreover, in appropriate conditions, their entrapment in reversed micelles has the parallel advantage of giving nanosized products, thus being considered a novel method to synthesize nanoparticles. The interest in nanoparticle synthesis is justified by the fact that nanoparticle properties can be very different from those of the bulk material, and so it is an alternative way to open new possibilities in the design of materials with new properties. There are two main reasons for nanoparticles to have such peculiar properties.

(i) In nanoparticles, the surface-to-volume ratio is much higher than in bulk material. So surface atoms, which are known to be in a different energetic state than the bulk atoms, make a distinct and consistent contribution to the total free energy. Hence, this causes changes in the thermodynamic properties such as melting temperature[10] and solid−solid-phase transition pressure.[11]

(ii) Even the intrinsic properties of nanocrystals are affected by quantum size effects. These effects arise from a systematic variation in the density of electronic energy levels with reducing the crystal size. In fact it is well know that the lower the number of atoms composing the nanocrystal, the lower the density of electronic states, the narrower the bandwidth, and the higher the energy gap. These transformations in the electronic structure imply a change in the chemical properties as ionization and redox potentials,[8] as well as photophysical and electric properties.[12−14]

For these reasons the reduction of an already known material to the state of nanoparticles is an alternative way to synthesize and design advanced materials with tuneable physical and chemical properties. Furthermore, the use of nanosized materials is a natural answer to the recent technological need to realize miniaturized devices, such as nano-sensors, nano-carriers, and nano-machines.[15]

In this contribution we investigated the synthesis of ZnS nanoparticles (Q dots) by solid−solid reaction between ultra-

* Corresponding author. E-mail: turco@unipa.it.
[†] Università degli Studi di Palermo.
[‡] ISMN, Istituto per lo Studio dei Materiali Nanostrutturati.

10.1021/jp021223+ CCC: $25.00
Published on Web 12/10/2002

small nanoparticles of Na_2S and $ZnSO_4$ dispersed in AOT/*n*-heptane solutions. The feasibility of such a reaction at fixed ZnS-to-AOT molar ratio (Rs) has been recently tested and the preliminary results are reported in a previous paper of which the present one constitutes the logical continuation.[16] The interest in ZnS nanoparticles is justified by their current and potential application in modern technology as seeds for other substance growth[17] or as a photocatalyst for CO_2 reduction,[18] and for their peculiar physicochemical properties.[19,20] Moreover, it must be stressed that, apart from the specific interest in ZnS nanoparticles, the same synthetic route could be used for a wide range of substances.

Structural and photophysical properties of ZnS-containing AOT reversed micelles reported in this work have been achieved as a function of Rs ($0 \leq Rs \leq 0.075$) and AOT concentration ($0.025 \leq [AOT] \leq 0.45$ mol kg^{-1}) by small-angle X-ray scattering (SAXS) and UV spectrophotometry. The analysis of these data will point out that the synthetic route based on the solid−solid reaction between $ZnSO_4$ and Na_2S nanoparticles possesses specific advantages with respect to the classical synthesis of ZnS by microemulsions.[21] From a different perspective, unexpected experimental evidence, suggesting that ZnS nanoparticle energy gap does not solely depend on the size, will be presented.

Experimental Part

Materials. Sodium bis(2-ethylhexyl)sulfosuccinate (aerosol-OT, AOT Sigma 98%) was stored in a desiccator and used after at least one week. *n*-Heptane (Aldrich 99% spectrophotometric grade), zinc sulfate monohydrate (Carlo Erba 98%, Analyticals), and sodium sulfide nonahydrate (Sigma ≥ 98%, ACS Reagent) were used as received. Bidistilled water was used in all experiments.

Method. AOT/*n*-heptane solutions containing ZnS nanoparticles were prepared by simply mixing equal weights of AOT/*n*-heptane solutions containing $ZnSO_4$ and Na_2S nanoparticles, respectively. The two reacting solutions had the same salt and surfactant concentrations, that were time by time opportunely chosen to give the desired final ZnS-to-AOT molar ratio (Rs). The details on the preparation of such nanoparticle-containing solutions and information on their structural properties are given in ref 16.

All liquid samples filled a dry quartz cell of suitable depth (from 0.2 to 2 mm, depending on the salt and surfactant concentrations) which was safely blocked and kept at thermostated room temperature (22 ± 1 °C) for the whole UV spectrophotometric investigation. An AOT/*n*-heptane solution at the same surfactant concentration was used as a blank. Measurements were carried out recording UV spectra in the wavelength range of 200−500 nm by a Perkin-Elmer Lambda 900 spectrometer as a function of time starting immediately after the mixing process. A NIR spectrum was also recorded for each sample in the 1800−2200 nm range to check the amount of residual water, which was found to be always less than 0.3 molecules for each AOT molecule.

The SAXS patterns have been recorded by a laboratory instrumentation consisting of a Philips PW 1830 X-ray generator providing Cu Kα, Ni-filtered ($\lambda = 1.5418$ Å) radiation with a Kratky small-angle camera in the "finite slit height" geometry equipped with a step scanning motor and a scintillation counter. Each scattering spectrum was subtracted by the cell + solvent contribution. Best-fit analyses were performed by the CERN minimization program called MINUITS. For each sample, SAXS spectra were recorded at various times, starting immediately after the mixing process. Only for the sample at [AOT] = 0.45 mol kg^{-1}, SAXS measurements were carried out after dilution with *n*-heptane to a final [AOT] = 0.1 mol kg^{-1}. This was necessary because the spectra of the undiluted sample showed scattering center interactions.

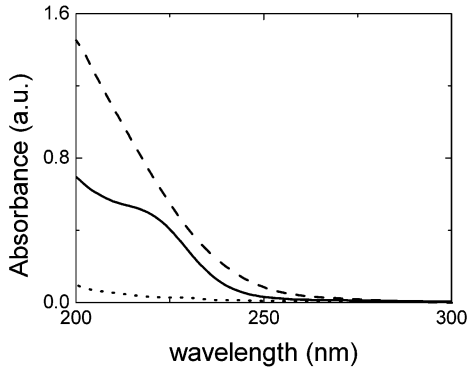

Figure 1. Typical UV spectra of salt-containing resuspensions at [AOT] = 0.025 mol kg^{-1} (Na_2S, dashed line; $ZnSO_4$, dotted line; ZnS at Rs = 0.060, continuous line).

Preparation of the ZnS nanoparticles/surfactant composites has been done by keeping the ZnS-containing AOT/*n*-heptane solution in a desiccator connected to a diaphragm vacuum pump (MZ2C, Vacuubrand). We tried to keep the evaporation time as short as possible to reduce the risk of any possible ZnS structural modification such as coalescence/agglomeration to the minimum. In this condition no change in the optical properties has been found to occur during the evaporation time.

Results and Discussion

Figure 1 shows a typical UV spectrum of a solution at Rs = 0.060 and [AOT] = 0.025 mol kg^{-1} prepared by mixing equal weights of two AOT/*n*-heptane solutions containing $ZnSO_4$ and Na_2S, respectively. This spectrum was recorded immediately after the mixing process and the UV spectra of the two $ZnSO_4$/AOT/*n*-heptane and Na_2S/AOT/*n*-heptane solutions are shown in the same graph as references. A new absorption band centered at about 220 nm can be noted in the spectrum of the mix. According to the literature, this band can be ascribed to the first excitonic absorption of ZnS, thus revealing the presence of such material in the mix.[22] Moreover, fast spectra recording showed that this band is already well-developed one minute after the mixing process, suggesting that complete ZnS nanoparticle formation takes place in a time shorter than one minute. It is also worth noting that this band is constituted by (i) a not well resolved peak located at shorter wavelengths than that of bulk ZnS (about 330 nm) clearly revealing that ZnS is nanosized,[22,23] and (ii) a tail of a more intense absorption occurring at shorter wavelengths due to higher energy electronic transitions as observable in low band gap semiconductor nanoparticles.[24,25]

Another striking feature of this band is its evolution with time. This is shown in Figure 2 where UV spectra collected at different times are reported. It can be noted that the peak shifts to longer wavelengths and the absorbance at the peak maximum is practically time-independent. This phenomenon is more marked in the first few hours after the mixing process and becomes slower and slower with time, tending to vanish in a period of 3 days. According to the literature the red shift of the absorption band with time could be rationalized by invoking a growth process of the ZnS nanoparticles similar to that occurring in the synthesis by microemulsions.[21] In fact a correlation has been found between the position (λ_{max}, nm) of the maximum of the absorption band and the size of the nanocrystal (d_{ZnS}, Å)

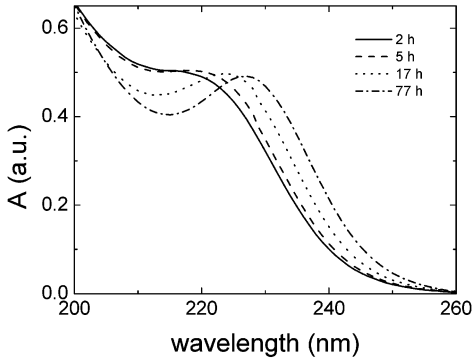

Figure 2. Typical time evolution of the UV spectrum of ZnS nanoparticles dispersed in AOT/*n*-heptane solution ([AOT] = 0.025 mol kg^{-1}, Rs = 0.060).

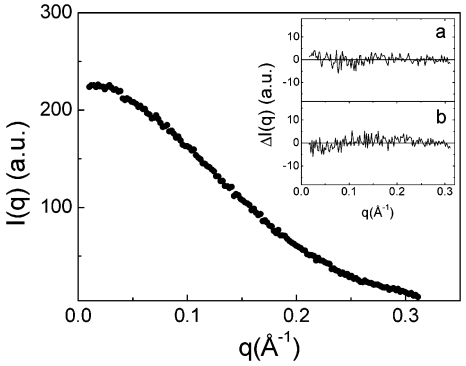

Figure 3. SAXS pattern of AOT reversed micelles containing ZnS nanoparticles at [AOT] = 0.10 mol kg^{-1} and Rs = 0.060 recorded immediately after the mixing process. The inserts show its difference with the diffractograms collected after 24 h (a) and 70 h (b).

described by the relation[21,26]

$$\lambda_{max} = 186.7 d_{ZnS}^{0.13} \quad (1)$$

To check whether the change in the photophysical properties with time arises from a growth process, we performed a small-angle X-ray scattering (SAXS) study of all the samples at different times. As an example, Figure 3 reports the SAXS pattern of a sample at [AOT] = 0.10 mol kg^{-1} and Rs = 0.060 recorded immediately after the mixing process, and the inserts show the difference spectra with the diffractogram collected after 24 h (a) and after 70 h (b). It clearly appears that no significant difference is observable in a period of 3 days. Since the SAXS profile is sensitive to size, shape, and polydispersity of ZnS-containing AOT reversed micellar cores,[27,28] this finding indicates that no significant time dependence of these parameters occurs and indirectly it leads to the hypothesis that it is not a nanoparticle growth process that causes the observed change in the photophysical properties with time but another factor, such as a slow atomic rearrangement taking place after the fast ZnS nanoparticle formation, must be considered.

SAXS Data Analysis. Further information on the size and polydispersity of ZnS-containing reversed micelles was obtained by a quantitative analysis of the SAXS patterns. All SAXS data, some of them are reported as representative in Figure 4 a and b, were found to be well-described by a model of not-interacting polydisperse homogeneous scattering spheres. In particular, the smeared spectra $I(q)$ were fitted with the equation

$$I(q) \propto \int_{-\infty}^{\infty} P(t) \int_{0}^{\infty} n(r) F^2(x)\, dr\, dt \quad (2)$$

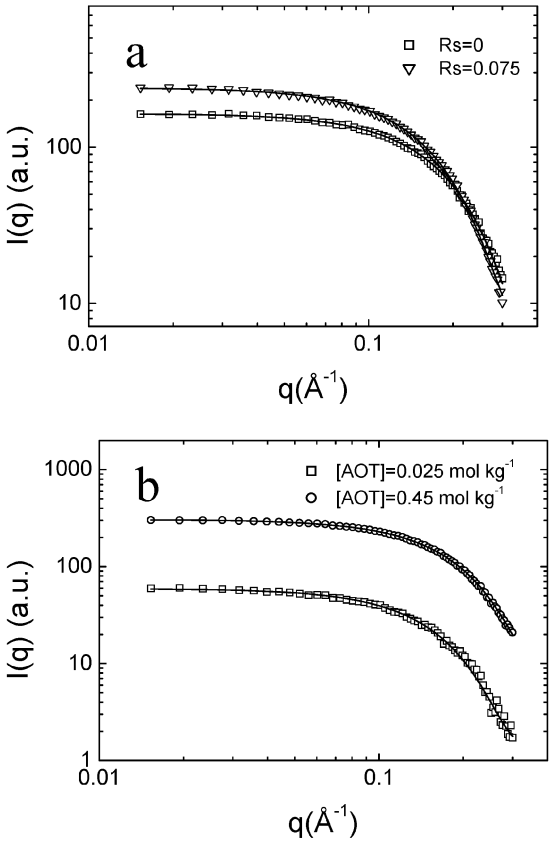

Figure 4. Representative SAXS experimental data and fitting curves for samples at [AOT] = 0.10 mol kg^{-1} (a) and Rs = 0.060 (b).

In this equation, q is the elastic scattering vector, t is a variable defined along the length of the line shaped primary X-ray beam, $P(t)$ is its intensity distribution function,[29] $F(x)$ is the form factor of a sphere of radius r given by

$$F(x) \propto \frac{\sin(x) - x\cos(x)}{x^3} r^3 \quad (3)$$

where $x = r(q^2 + t^2)^{1/2}$ and $n(r)$, the size distribution function, has been assumed to be the Weibull equation

$$n(r) \propto \left(\frac{r}{r^\circ}\right)^{b-1} \exp\left[-\left(\frac{r}{r^\circ}\right)^b\right] \quad (4)$$

In eq 4, b is a parameter controlling the shape of the size distribution function and r° is a parameter related to the sphere mean diameter d_m through the Γ function by

$$d_m = 2r^\circ \Gamma\left(\frac{b+1}{b}\right) \quad (5)$$

The Weibull equation was chosen to describe the size distribution function because it is very versatile since it represents a localized distribution around the mean value d_m, but it reduces to a simple exponential behavior when the parameter b takes the value of 1. Moreover, the parameter b, governing the shape of the size distribution function, is a quantitative descriptor of the size polydispersity.

It is important to point out that small-angle X-ray scattering originates from the contrast between adjacent regions with different electron densities. Figure 5 shows the electron density profile of a ZnS/AOT/*n*-heptane micelle[27] and it clearly reveals that the main electron density discontinuity lies in the surfactant polar head-aliphatic chain's ideal surface. So the scattering

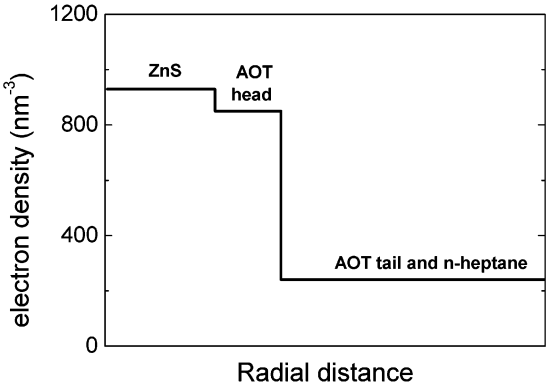

Figure 5. Electron density profile for a ZnS-containing AOT reversed micelle.

TABLE 1: Fitting Parameters Derived from SAXS Data as a Function of Rs and AOT Concentration

Rs	[AOT] (mol kg^{-1})	b	d_m (Å)
0	0.10	16	20.7
0.045	0.10	16	21.8
0.060	0.10	12	22.9
0.075	0.10	9	23.0
0.060	0.025	12	26.1
0.060	0.45	11	21.6

homogeneous spheres of the model represent the ZnS-containing micellar cores and consequently d_m must be interpreted as their mean diameter.

The fitting curves of the experimental data shown in Figure 4a and b are reported as continuous lines in the same graph. The fine agreement between the experimental points and the fitting curves strongly suggests the validity of the model. The derived parameters d_m and b are reported in Table 1 and the corresponding diameter distribution functions $n(d)$ of ZnS-containing AOT reversed micellar cores are shown in Figure 6a and b.

The observed dependence of the micellar core mean diameter on Rs at constant [AOT] can be easily rationalized by considering that ZnS, owing to its hydrophilic nature and insolubility in pure *n*-heptane, is all localized in the micellar core of AOT reversed micelles: the higher the salt-to-AOT molar ratio, the more the salt contained in the micelles and the higher their mean diameter. It is worth noting that also polydispersity increases, suggesting that the salt is not uniformly distributed among all the reversed micelles. On the other hand it can be noted that, at fixed Rs, the micellar core polydispersity does not depend on AOT concentration while the mean diameter does. The dependence of the mean size of the micellar core on the AOT concentration suggests that at lower [AOT] there is a lower material exchange rate between AOT reversed micelles containing $ZnSO_4$ and Na_2S nanoparticles, leading to a lower number of ZnS nuclei and, consequently, to bigger nanoparticles. Some additional comments are to be made:

(i) although it is not possible with our instrumentation to directly measure the ZnS nanoparticle diameter, the very slight increase in the micellar core diameter owing to the presence of ZnS entrapped in reversed micelles (see Table 1 and Figure 6a and b) suggests that ZnS nanoparticles must be very small (diameter of a few angstroms): they would be so small that it would be impossible for them to be synthesized by other synthetic methods.

(ii) in our experimental conditions, ZnS concentration is about 1 order of magnitude higher than that typically reached by means of w/o microemulsions. This partially solves the problems arising from the use of samples with low nanoparticle density and so this is a specific advantage of the present method of synthesis.

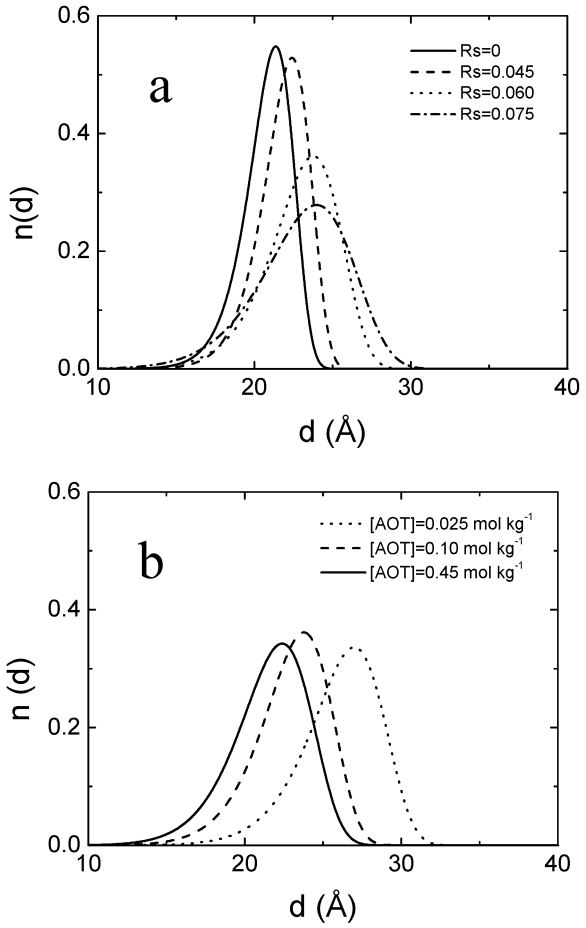

Figure 6. Size distribution functions of the micellar core for samples at various Rs values and [AOT] = 0.10 mol kg^{-1} (a); and at various [AOT] and Rs = 0.060 (b).

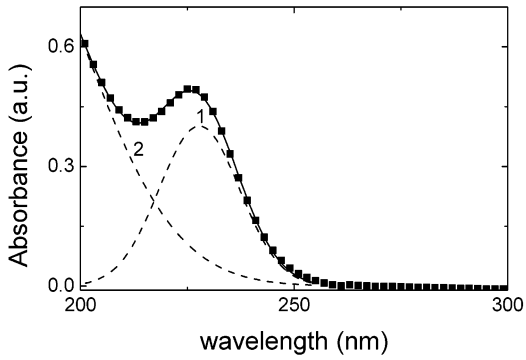

Figure 7. Representative Gaussian deconvolution of the UV spectrum of an AOT/*n*-heptane solution containing ZnS nanoparticles at [AOT] = 0.025 mol kg^{-1} and Rs = 0.060.

UV Spectra Analysis. A quantitative investigation of the change of the UV absorption band with time requires the exact determination of the maximum of absorption for each spectrum. This was achieved by deconvolution of the UV absorption feature in two Gaussian curves as shown in Figure 7 where a typical result, referring to a sample at Rs = 0.060 and [AOT] = 0.025 mol kg^{-1}, is reported. The goodness of the fit was always very high, the correlation coefficient generally being greater than 0.9990. This involves that the spin−orbit coupling

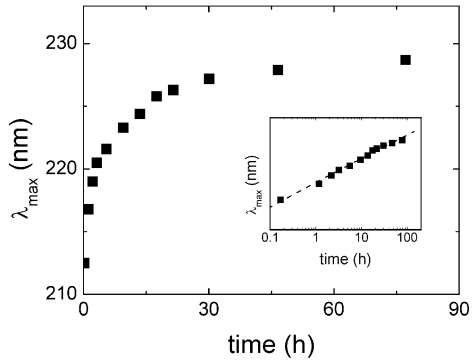

Figure 8. Typical time dependence of λ_{max}. The insert shows the trend in a log−log scale.

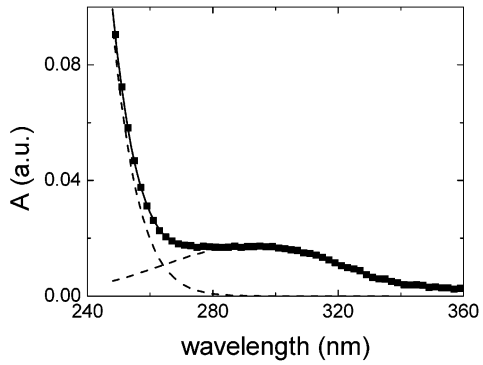

Figure 9. Shoulder and Gaussian fitting curves of the first excitonic transition band in a sample at [AOT] = 0.10 mol kg^{-1} and Rs = 0.060.

leading to a more structured band and already observed in ZnS nanoparticles[22] (diameter ≈ 21 Å) is so small to be considered negligible in our systems.

The Gaussian centered at higher wavelengths (Gaussian 1 in Figure 7) should now adequately describe the first excitonic transition, being free from the interference of the tail of the more intense absorption band at shorter wavelengths (Gaussian 2 in Figure 7) due to higher energy electronic transitions. As it can be seen, the maximum of the high-energy absorption band occurs at wavelengths shorter than 200 nm, i.e., out of the range accessible by our instrument. This implies that its exact position cannot be determined and so we were forced to focus our attention only on Gaussian 1 and in particular on the time evolution of its position (λ_{max}).

A typical trend of λ_{max} as a function of time (t in hours) is shown in Figure 8: λ_{max} increases with time at a rate that becomes slower and slower, tending to reach a limit value at long times (about 3 days). The insert in Figure 8 shows the data in a log−log scale, and the linear trend clearly reveals that λ_{max} follows the law

$$\lambda_{max} = At^B \quad (6)$$

This behavior was observed for all samples and, more interestingly, the constants A and B derived by best-fit analysis are nearly constant and equal to 2.3 ± 0.3 and 0.010 ± 0.003, respectively. This finding shows that the process probed by UV spectroscopy is Rs- and [AOT]-independent and it could be tentatively attributed to an internal ZnS nanoparticle rearrangement.

A careful perusal of the UV spectra reveals the presence of a very low intensity shoulder at the lower frequency side of the absorption band. This additional feature, shown in Figure 9, was already observed by Li et al.[30] and was supposed to be

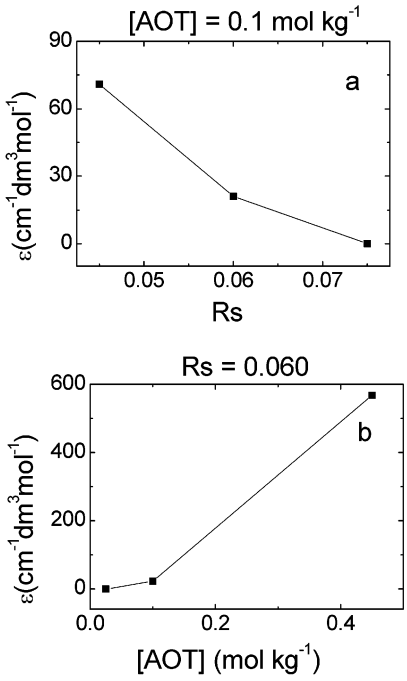

Figure 10. The molar extinction coefficient (ϵ) of the shoulder of the first excitonic transition at constant [AOT] as a function of Rs (a), and at constant Rs as a function of [AOT] (b).

caused by sulfur vacancy defects. Both position and intensity of the shoulder were found to be time independent. Since the intensity of this peak is a probe of the amount of such defects, we reported in Figure 10 the molar extinction coefficient (ϵ) at the shoulder maximum as a function of Rs (a) and surfactant concentration (b). ϵ was derived through the usual deconvolution of the UV absorption feature in the 240−340 nm range in two Gaussian curves. Figure 10 shows that [AOT] and Rs are suitable parameters controlling the amount of sulfur vacancy defects. This is because [AOT] and Rs govern the inter-micellar collision rate and consequently the mechanism itself involved in the formation of ZnS nanoparticle nuclei and their subsequent growth.

Incidentally, it must be stressed that the modulation of the amount of this type of defect in ZnS nanoparticles is very important because most semiconductor properties are highly dependent on the nature and amount of structural defects. Moreover, since Tata et al. in their study on CdS nanoparticles[31] have ascertained the role of water as quenching agent of nanoparticle luminescence, the virtually water-free ZnS nanoparticles synthesized by the present solid−solid reaction are expected to exhibit enhanced luminescence properties.

To shed more light on the time dependence of ZnS nanoparticle's photophysical properties, we investigated the time evolution of the UV spectrum of the composite obtained by fast and complete evaporation of the organic solvent at room temperature. Figure 11 reports the comparison, at different times, between the UV spectrum of ZnS nanoparticles dispersed in AOT/*n*-heptane solution and that of AOT/ZnS composite (Rs = 0.060). AOT/ZnS composites spectra were carried out on the resuspension obtained by fast dispersion of the composite in *n*-heptane. It is worth noting that the red-shift with time occurs also when ZnS nanoparticles are hosted in the solid AOT matrix, thus excluding that it can be somehow assisted by nanoparticle diffusion process or material exchange among nanoparticles, these processes all being frozen in the solid state. More interestingly, the kinetics is the same as that already observed for liquid samples. This is a strong proof in favor of the

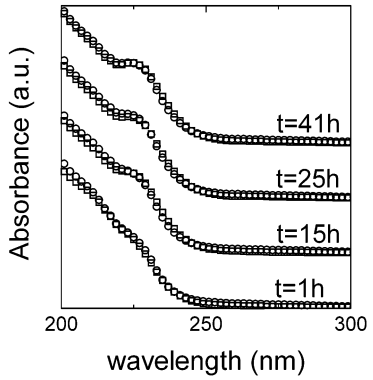

Figure 11. Comparison between the UV spectra of ZnS nanoparticles dispersed in AOT/*n*-heptane solution (squares) and of resuspended AOT/ZnS composite (circles) at various times (*t*).

hypothesis of a ZnS nanoparticle atomic rearrangement like a surface relaxation or a slow transition from an amorphous structure to a more ordered one, similarly to that occurring in glasses.

Conclusions

We exploited for the first time a novel solid−solid reaction between Na_2S and $ZnSO_4$ nanoparticles in the liquid phase to give ultra-small ZnS Q dots. This method of synthesis allows a modulation of structural and photophysical properties by changing salt and surfactant concentrations. All experiments showed that ZnS nanoparticle formation is fast and complete. Nanoparticle size was found to be very small (a few angstroms) and their concentration higher than that achieved through other synthetic routes. The coupled analysis of SAXS and UV spectra suggested that the energy gap does not uniquely depend on the nanoparticle size, but one more factor such as atomic arrangement could be involved. To clarify the microscopic factors involved, we plan to perform WAXS, EXAFS, and XPS investigations on our systems.

Acknowledgment. Financial support from MIUR 60% is gratefully acknowledged.

References and Notes

(1) Epple, M.; Ebbinghaus, S.; Reller, A.; Gloistein, U.; Cammenga, H. K. *Thermochim. Acta* **1995**, *269/270*, 433, and references therein.

(2) Coville, N. J.; Cheng, L. *J. Organomet. Chem.* **1998**, *571*, 149, and references therein.

(3) Kraupp, G.; Schmeyers, J.; Boy, J. *Tetrahedron* **2000**, *56*, 6899.

(4) Lei, L.; Xin, X. *Thermochim. Acta* **1996**, *273*, 61.

(5) Jankowski, J.; Thomas, G.; Camby L. P. *Solid State Ionics* **1997**, *101*−*103*, 1321.

(6) Hesse, D.; Graff, A.; Senz, S.; Zakharov, N. D. *Ceram. Int.* **2000**, *26*, 753.

(7) Willson, R. J.; Beezer, A. E.; Mitchell, J. C. *Int. J. Pharm.* **1996**, *132*, 45.

(8) West, A. R. *Solid State Chemistry and Its Application*; John Wiley: New York, 1984.

(9) Eguchi, K.; Akasaka, N.; Mitsuyasu, H.; Nonaka, Y. *Solid State Ionics* **2000**, *135*, 589.

(10) Goldstain, A. N.; Echer, C. M.; Alivisatos, A. P. *Science* **1992**, *256*, 1425.

(11) Brus, L. E.; Harkless, J. A. W.; Stillinger, F. H. *J. Am. Chem. Soc.* **1996**, *118*, 4834, and references therein.

(12) Vogelsang, H.; Husberg, O.; von der Osten, W. *J. Lumin.* **2000**, *86*, 87.

(13) Schmid, G.; Bäumle, M.; Geerkens, M.; Heim, I.; Osemann, C.; Sawitowski, T. *Chem. Soc. Rev.* **1999**, *28*, 179, and references therein.

(14) Zhang J. Z. *J. Phys. Chem. B* **2000**, *104*, 7239.

(15) Drexler, K. E. *Nanosystems*; J. Wiley & Sons Inc.: New York, 1992.

(16) Calandra, P.; Longo, A.; Turco Liveri, V. *Colloid Polym. Sci.* **2001**, *279*, 1112.

(17) Kortan, A. R.; Hull, R.; Opila, R. L.; Bawendi, M. G.; Steigerwald, M. L.; Carroll, P. L.; Brus, L. E. *J. Am. Chem. Soc.* **1990**, *112*, 1327.

(18) Fujiwara, H.; Hosokawa, H.; Murakoshi, K.; Wada, Y.; Yanagida, S. *Langmuir* **1998**, *14*, 5154.

(19) Sooklal, K.; Cullum, B. S.; Angel, S. M.; Murphy, C. J. *J. Phys. Chem.* **1996**, *100*, 4551.

(20) Lin, C. H.; Chiou, B. S.; Chang, C. H.; Lin, J. D. *J. Mater. Sci.: Mater. Electron.* **2002**, *13*, 1.

(21) Calandra, P.; Goffredi, M.; Turco Liveri, V. *Colloids Surf., A* **1999**, *160*, 9.

(22) Chestnoy, N.; Hull, R.; Brus, L. E. *J. Chem. Phys.* **1986**, *85* (4), 2237.

(23) Vogel, W. *Langmuir* **2000**, *16*, 2032, and references therein.

(24) Brus, L. E. *J. Phys. Chem.* **1986**, *90*, 2555.

(25) Henglein, A. *Chem. Rev.* **1989**, *89*, 1861.

(26) Nakaoka, Y.; Nosaka, Y. *Langmuir* **1997**, *13*, 708.

(27) North, A. N.; Dore, J. C.; McDonald, J. A.; Robinson, B. H.; Heenan, R. K.; Howe, A. M. *Colloids Surf.* **1986**, *19*, 21.

(28) Mackeben, S.; Muller-Goymann, C. C. *Int. J. Pharm.* **2000**, *196*, 207.

(29) Ruland, W. *J. Appl. Crystallogr.* **1974**, *7*, 383.

(30) Li, Y.; Ding, Y.; Zhang, Y.; Quian, Y. *J. Phys. Chem. Solids* **1999**, *60*, 13.

(31) Tata, M.; Banerjee, S.; John, V. T.; Waguespack, Y.; McPherson, G. L. *Colloids Surf., A* **1997**, *127*, 39.